Electronic Supplementary Material (ESI) for Journal of Materials Chemistry C.
This journal is © The Royal Society of Chemistry 2022

Electronic Supplementary Information

An efficient cooling solution with 3D interconnected graphene architectures for passive heat dissipation

Yangziwan Weng,[a] Sicheng Wu,[a] Linbin Wang,[a] Weiyun Zhao,*[a] Yi Jiang*[a] and Yuan Deng[ab]

a. *Key Laboratory of Intelligent Sensing Materials and Chip Integration Technology of Zhejiang Province, Hangzhou Innovation Institute of Beihang University, Hangzhou 310051, China*
b. *Research Institute for Frontier Science, Beihang University, Beijing, 100083, China.*

E-mail addresses: zhaowyhz@buaa.edu.cn; jiangyi102503@hotmail.com

Cooling Efficiency Measurement

The cooling efficiency (δ) was calculated using the following equation.[1]

$$\delta = \frac{\Delta T}{\Delta T_c} \tag{S1}$$

Where δ is the cooling efficiency (%), ΔT represents the reduction of the equilibrium temperature (K) and ΔT_c is temperature change of the copper block without any cover under continuous heating (K).

Calculation of Thermal Emissivity

Surface long-wave infrared emission emissivity (LWIR) was defined and calculated as:[2, 3]

$$\varepsilon(LWIR) = \frac{\int_{8\,\mu m}^{13\,\mu m} I_{BB}(T,\ \lambda)\varepsilon(\lambda)d\lambda}{\int_{8\,\mu m}^{13\,\mu m} I_{BB}(T,\ \lambda)d\lambda} \tag{S2}$$

Where λ is the wavelength and 8-13 μm bounds represent the LWIR atmospheric transmittance window, $I_{BB}(\lambda)$ is the spectral intensity emitted by a blackbody (assumed at 25˚C) and $\varepsilon(\lambda)$ is the surface's spectral emissivity $\varepsilon(\lambda)$=1-$R(\lambda)$.

Supplementary Figures

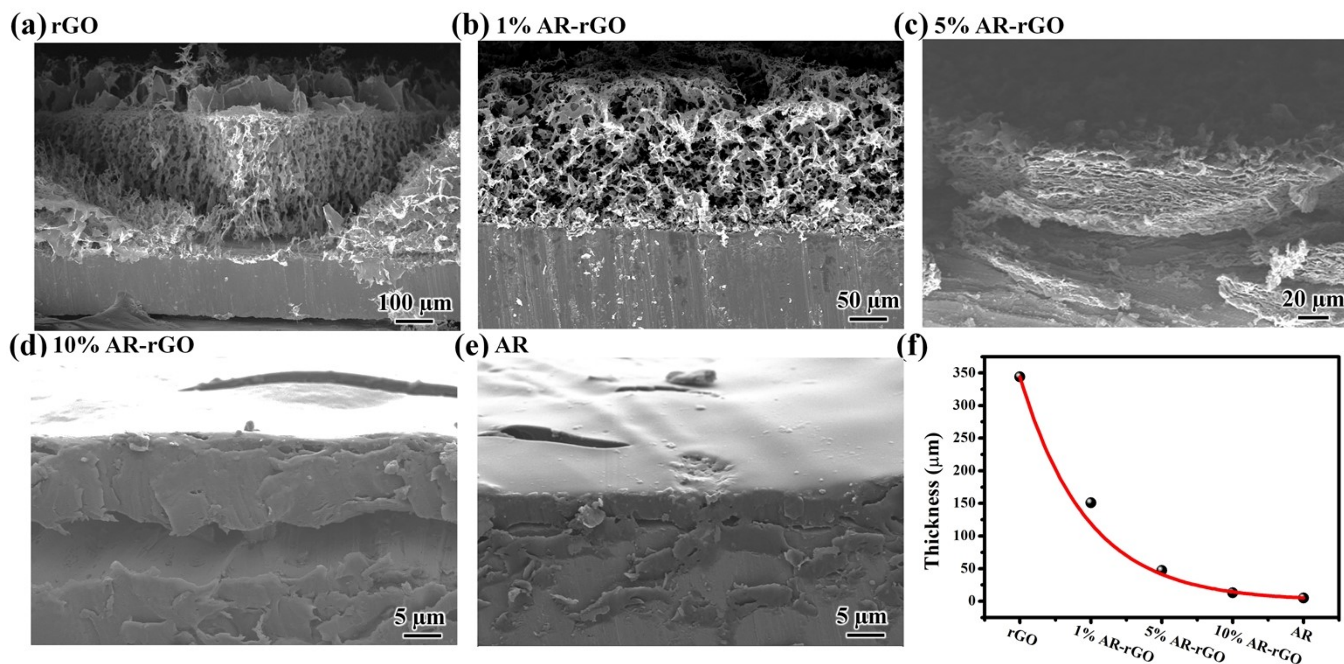

Figure S1. Cross-sectional SEM images of (a) rGO, (b) 1% AR-rGO, (c) 5% AR-rGO, (d) 10% AR-rGO and (e) AR. (f) The corresponding thickness of each sample.

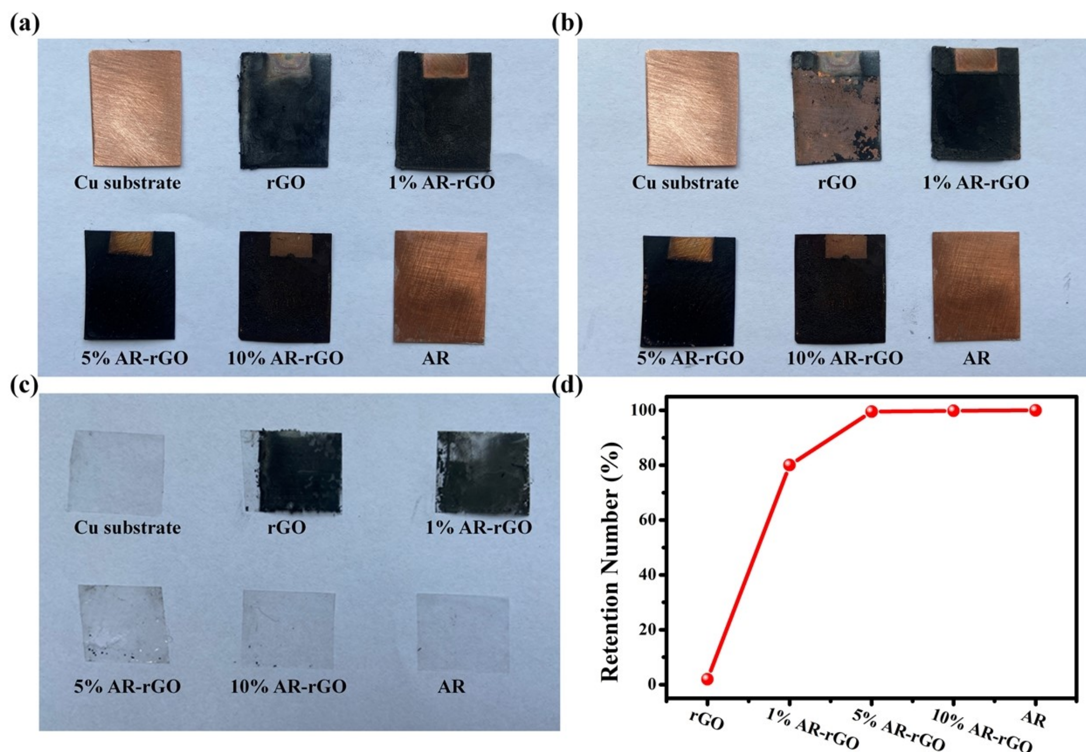

Figure S2. Samples for peel test. Optical images of Cu sheet, rGO, *x*% AR-rGO and AR (a) before and (b) after tape tests. (c) A photograph of the 3M tape and (d) the retention of samples on the Cu sheet after tape rests.

Measuring adhesion by a tape test

A commercial transparent 3M tape was placed on the top of the sample and smoothed by a roller. After full contact for 2 min, the tape was rapidly removed by seizing the free end. Figures S2a-b show the optical images of test samples before and after tape tests.

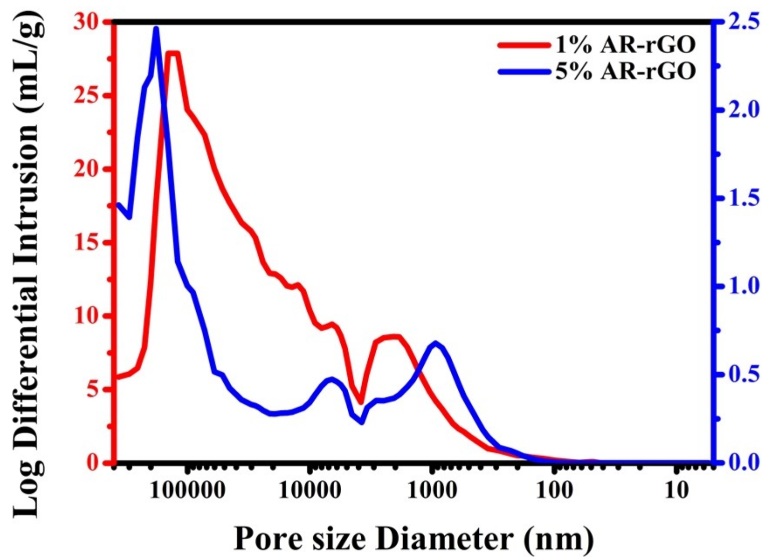

Figure S3. The pore size distributions of 1% and 5% AR-rGO obtained from mercury injection apparatus measurements.

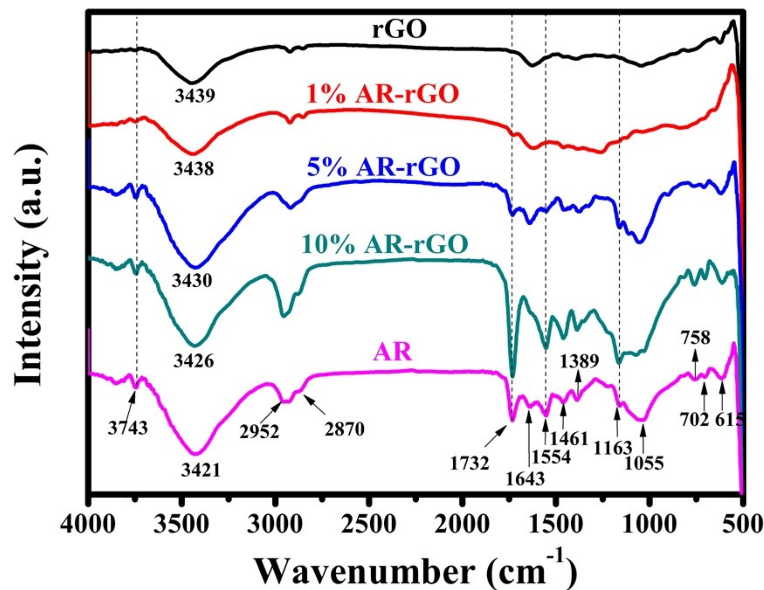

Figure S4. FTIR absorption spectra of rGO, *x*% AR-rGO and AR.

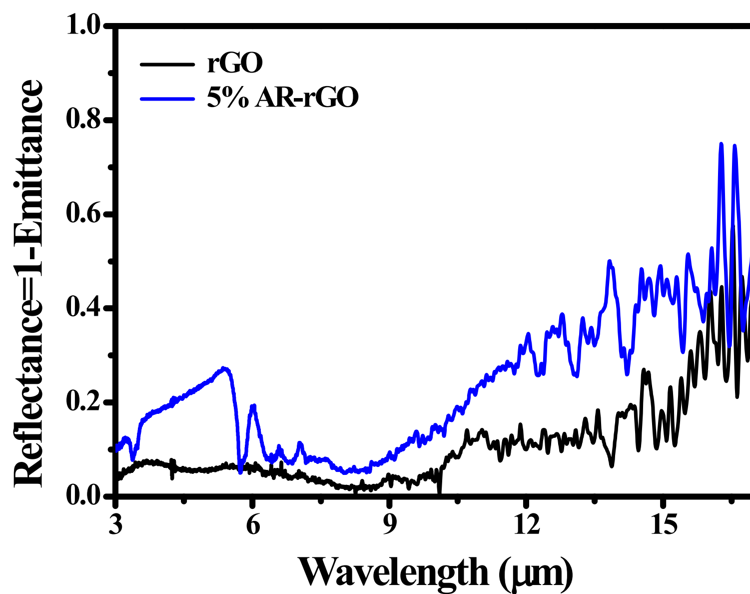

Figure S5. Spectral reflectance ($\varepsilon(\lambda)$=1-$R(\lambda)$) of rGO and 5% AR-rGO presented against the LWIR atmospheric transparency window.

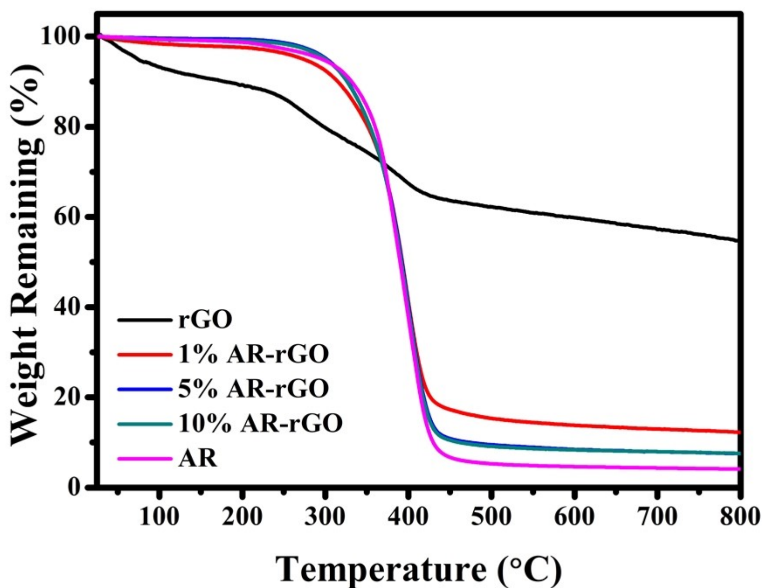

Figure S6. thermogravimetric analysis under N_2 environment.

Table S1. The weight remaining after thermogravimetric tests and calculated rGO contents of rGO, *x*% AR-rGO and AR.

Sample	Weight remaining (%)	Calculated content of rGO (%)
rGO	54.7	100.0
1% AR-rGO	12.2	16.0
5% AR-rGO	7.6	6.9
10% AR-rGO	7.5	6.7
AR	4.1	0.0

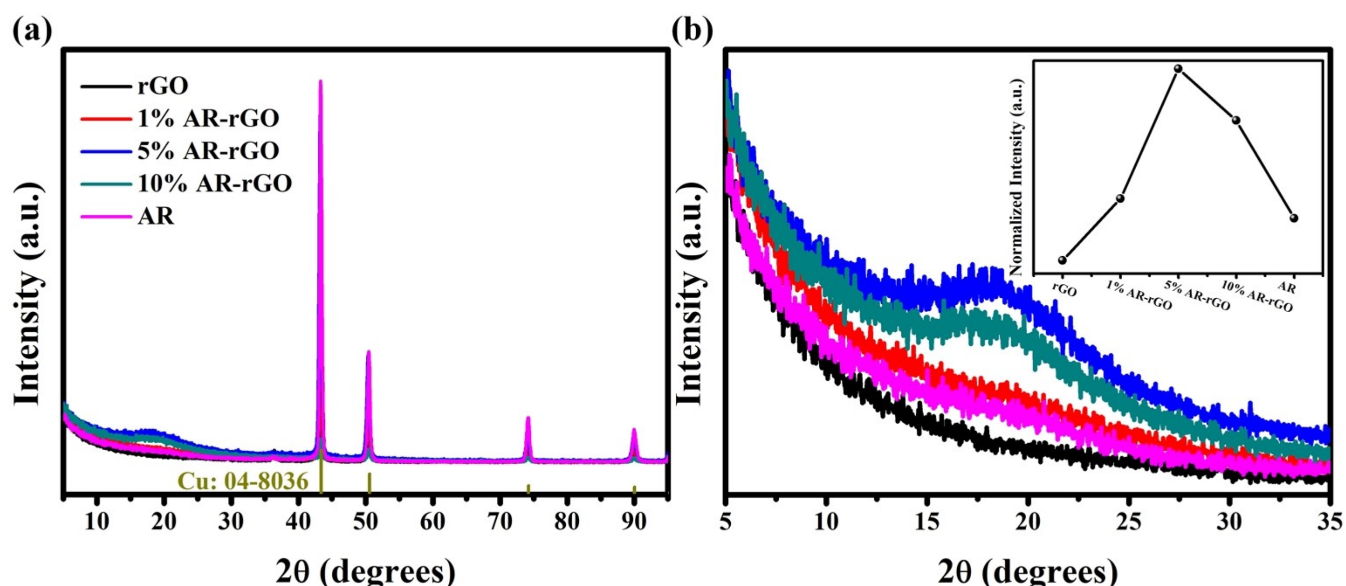

Figure S7. XRD with different magnifications of rGO, *x*% AR-rGO and AR. The inset in (b) shows the intensities of graphitized carbon (002) peaks in series samples.

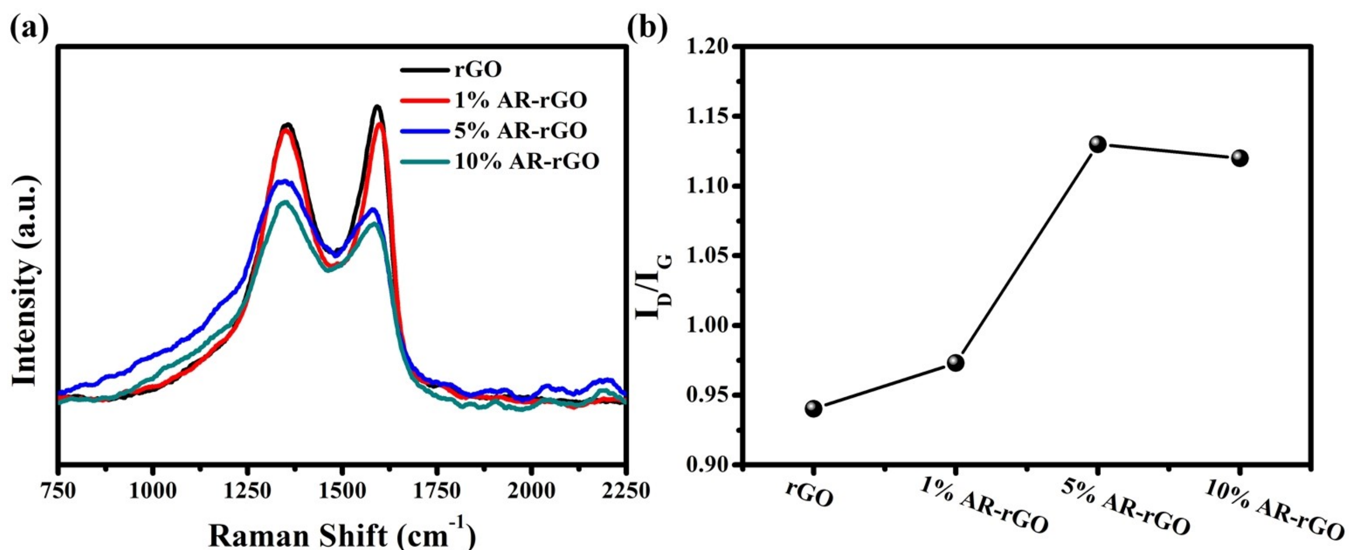

Figure S8. (a) Raman spectra of the rGO and *x*% AR-rGO and (b) corresponding I_D/I_G ratios.

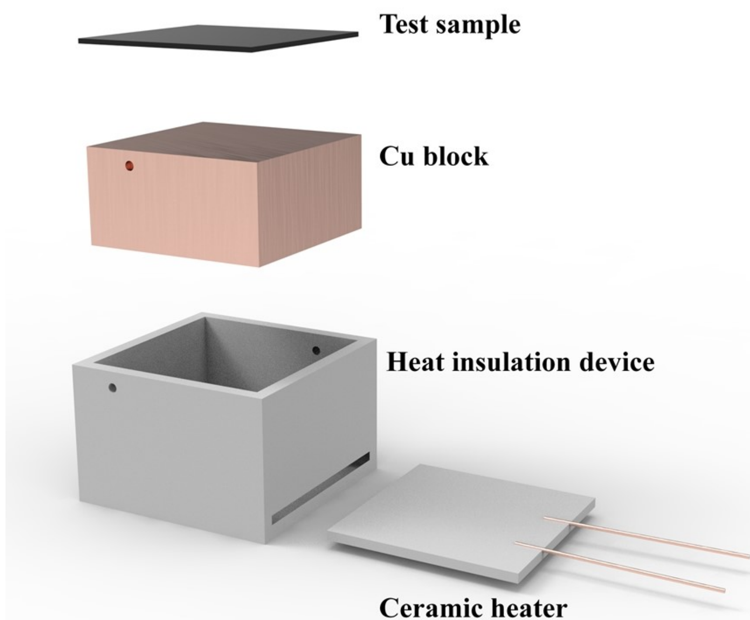

Figure S9. Schematic diagram of dissipated heat measurement setup upon heating using ceramic heater and measuring temperature of the test point by thermoelectric couple.

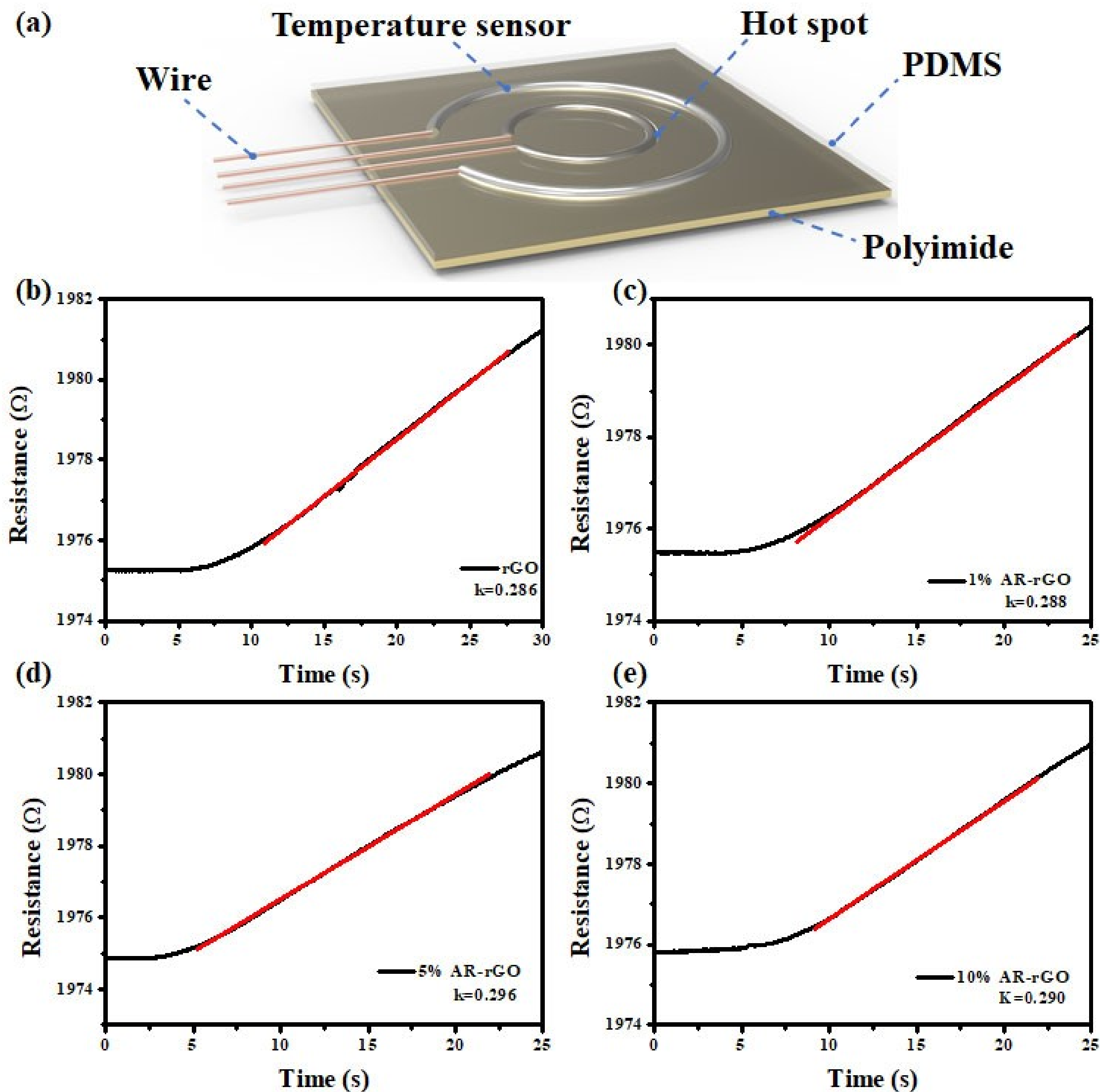

Figure S10. (a) Schematic diagram of thermal transmission measurement setup. Dynamic resistance responses of the temperature sensor when rGO (b), 1% AR-rGO (c), 5% AR-rGO (d), 10% AR-rGO (e) was exposed to it, respectively.

Thermal Transmission Measurement Device Fabrication

Thermal transmission capacity of the samples was measured by the measurement setup as shown in Figure S9. This electronic sensory system was composed of three layers, including polyimide (PI) substrate, sensing units and polydimethylsiloxane (PDMS) film. Sensing units comprise two nickel (Ni) thermosensitive rings. The inner ring with a resistance of 100 Ω is defined as a hot spot and the outer ring with a resistance of 2000 Ω is used as a temperature sensor. Under an equal applied voltage, the inner ring bears a higher electrical power and thereby is heated to be a hot spot, while a lower Joule heating is produced in the outer ring because of its larger resistance. When a sample is exposed to the hot spot, the

heat spreads evenly through the sample and thus the resistance of thermosensitive outer ring is changed. The better the thermal transmission ability of the sample is, the larger the variation of dynamic resistance is. Therefore, the slope of resistance-temperature curve can qualitatively evaluate the thermal transmission performance of a sample.

The fabrication of this device was according to a literature method with a few modifications.[4, 5] Briefly, Ni films were deposited and patterned on the PI substrate by vacuum thermal evaporation (ZHD400 system purchased from Beijing Technol Science Co., Ltd.), followed by annealing for 2 h at 200 ºC in a vacuum oven. Finally, a PDMS film was coated on the sensor by spun for encapsulation.

Table S2. Comparison of heat dissipation capability with 3D graphene composites reported in the literature.

Sample	LED temperature drop (ºC)	Ref.
rGO	16 ºC	6
3D kaolin/graphene	650 mA: 20 ºC	7
2D GNFs/1D MWCNTs/Al_2O_3	15 W: 21.3 ºC	8
Al_2O_3/rGO	1W: 5.6 ºC; 5 W: 14.0 ºC	9
PP/graphene composites	20 ºC	10
GNs/GF/natural rubber composite	29.8 ºC	11
Nanofibrillated Cellulose/MgO@rGO	8.4 ºC	12
rGO	1 W: 6.84 ºC; 5 W: 20.76 ºC	This work
5% AR-rGO	1 W: 11.75 ºC；5 W: 30.62 ºC	This work

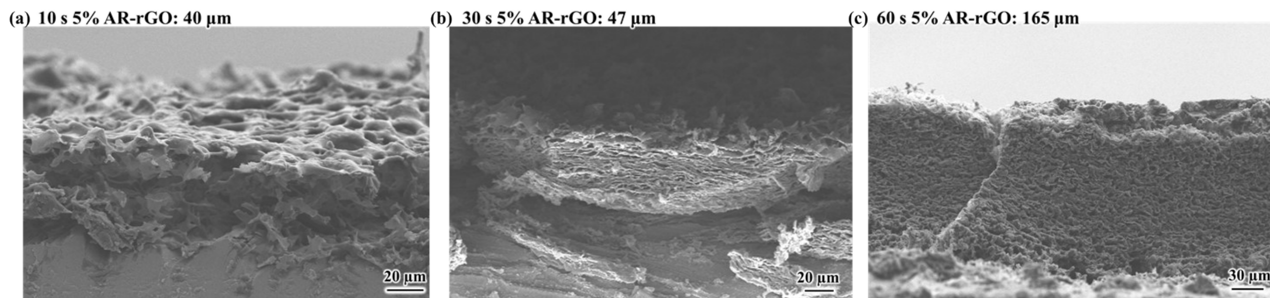

Figure S11. Cross-sectional SEM images of 5% AR-rGO under (a) 10 s, (b) 30 s and (c) 60 s deposition time.

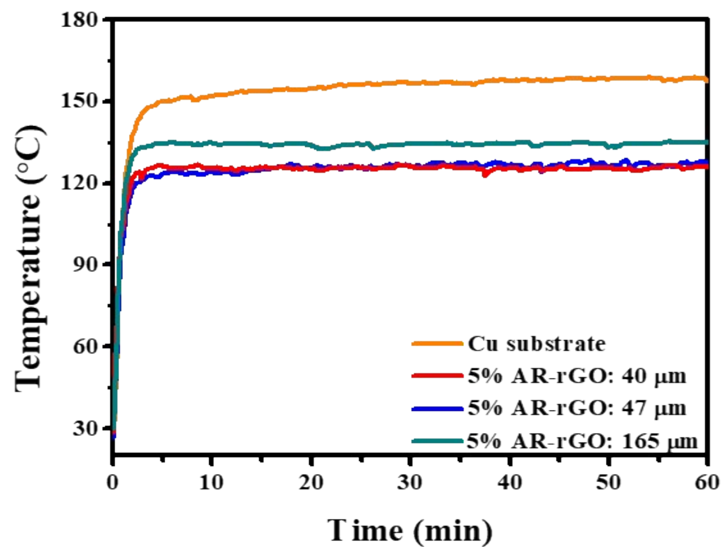

Figure S12. Temperature curves of 5W commercial LEDs chips with varying thickness 5% AR-rGO.

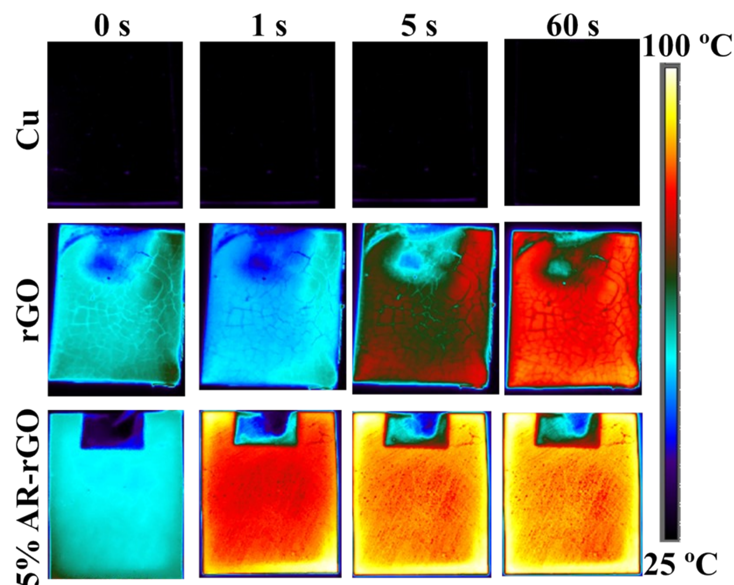

Figure S13. IR images of self-made heat sinks and Cu substrate on the heating platform.

References

1. Y. Zou, Y. Wang, S. Xu, T. Jin, D. Wei, J. Ouyang, D. Jia and Y. Zhou, *Chem. Eng. J.*, 2019, **362**, 638-649.
2. P. Li, A. Wang, J. Fan, Q. Kang, P. Jiang, H. Bao and X. Huang, *Adv. Funct. Mater.*, 2021, **32**, 2109542-2109551.
3. W. Yu, Z. Duan, G. Zhang, C. Liu and S. Fan, *Nano Lett.*, 2018, **18**, 1770-1776.
4. S. Zhao and R. Zhu, *Adv. Mater. Technol.*, 2018, **3**, 1800056-1800063.
5. G. Li and R. Zhu, *Adv. Mater. Technol.*, 2019, **4**, 1900602.
6. J. S. Lee, T. Kim, H. H. Lee and Y. H. Kim, *J. Mater. Chem. C*, 2018, **6**, 2515-2521
7. Q. Sun, J. Liu, Y. Peng, A. Wang, Z. Wu and M. Chen, *J. Alloys Compd.*, 2020, **817**, 152779.
8. C. Cheng, W. H. Shi, T. P. Teng and C. R. Yang, *Polymers*, 2022, **14**, 952-970.
9. Y. Zou, Y. Wang, H. Zhang, D. Wei, T. Jin, H. Wang, S. Liao, D. Jia and Y. Zhou, *Mater. Des.*, 2018, **157**, 130-140.
10. N. Song, D. Cao, X. Luo, Q. Wang, P. Ding and L. Shi, *Compos. Part A Appl. Sci. Manuf.*, 2020, **135**, 105912.
11. Z. Wu, C. Xu, C. Ma, Z. Liu, H. M. Cheng and W. Ren, *Adv. Mater.*, 2019, **31**, e1900199
12. M. Ma, L. Xu, L. Qiao, S. Chen, Y. Shi, H. He and X. Wang, *Chem. Eng. J.*, 2020, **392**, 123714-123722.